Hadron Distributions at Higher Rapidity Using the BRAHMS Forward Spectrometer

Bruce Moskowitz[a] *
for the BRAHMS Collaboration[b]

[a]Physics Department, Brookhaven National Laboratory,
Upton, New York 11973, U.S.A.

[b]BNL, CRN-Strasbourg, NBI-Copenhagen, CIAE-Beijing, NYU, Texas A&M,
UCSSL-Berkeley

Different conditions, and therefore different physics, are expected to exist over the range of rapidities at RHIC. The BRAHMS Forward Spectrometer will measure identified hadron distributions up to y=4, giving it a unique place in the RHIC experimental program.

1. WHY MAKE MEASUREMENTS AT HIGHER RAPIDITY?

The primary motivation for performing experiments at RHIC is to search for signs of the formation of a quark-gluon plasma. Regardless of whether such a state of matter is convincingly discovered or not, it is important that the basic conditions existing in RHIC collisions be well described in terms of energy and baryon density, thermodynamic and hydrodynamic properties, hadronization, etc. Since different conditions will certainly exist at different rapidities, experiments should investigate the regions of higher rapidity as well midrapidity.

2. SOFT PARTICLE SPECTRA

The dominant region of particle distributions from RHIC collisions is expected to be the "soft" part with transverse momentum $p_T < 2$ GeV/c. The QCD theory is highly non-perturbative in this regime of relatively large distances, but string models may be used to characterize particle production. Three popular models for nucleus-nucleus collisions, all of which are based in part on string theory and in part on scaling from p+p data, particularly from the CERN ISR ($\sqrt{s}$=24–63 GeV), are compared in Fig. 1. Plotted are the predictions of Fritiof[1], Venus[2] and RQMD[3] for the rapidity distributions of net baryons and of mesons from central Au+Au collisions at $\sqrt{s}$=200 GeV per nucleon pair. Note that the RQMD predictions for the net baryon distribution differ from those presented at Quark Matter '91[4] due to the correction of a computational error[5].

*This research was supported by the U.S. Department of Energy under contract no. DE-AC02-76CH00016.

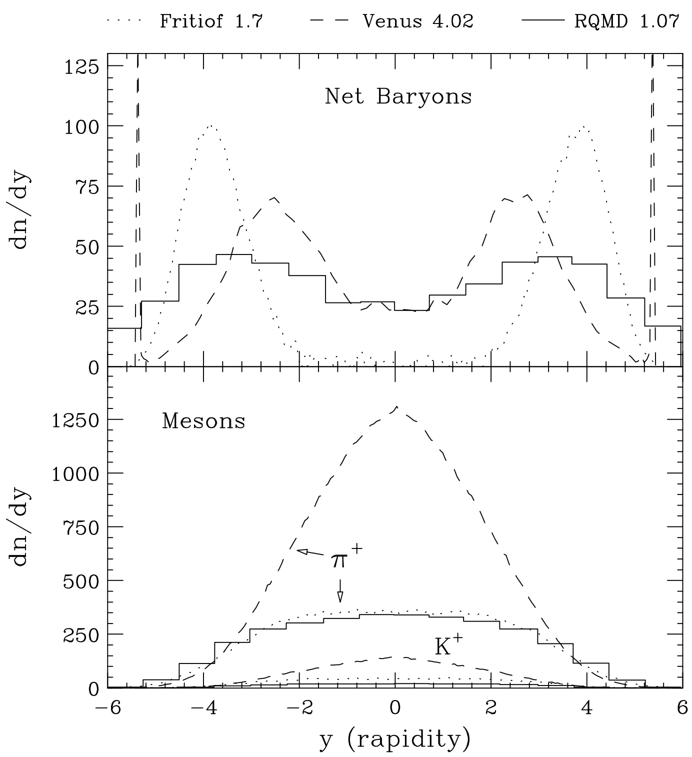

Figure 1. Rapidity distributions for net baryons (top panel) and mesons (bottom panel) from central Au+Au collisions at 200 GeV per nucleon pair as predicted by Fritiof 1.7 (dotted curves), Venus 4.02 (dashed) and RQMD 1.07 (solid, from Ref. [3]).

2.1. Baryon stopping

One of the most basic questions concerning RHIC is how high the net baryon density (i.e., the difference between baryons and antibaryons) will be in the central regions of Au+Au collisions. As seen in the top panel of Fig. 1, the net baryon dn/dy at midrapidity vanishes for Fritiof. Furthermore, Fritiof predicts the baryon "stopping power", i.e., the mean rapidity shift per projectile baryon, to be $<\Delta y>$=1.9 units. (Recall that the beam rapidity is $\pm$5.6.) By comparison, an analysis of fixed target data at $\sqrt{s}$=14 GeV yields $<\Delta y>$=0.95$\pm$0.15 for p+p and $<\Delta y>$=1.9$\pm$0.3 for p+Pb[6]. A new, improved compilation of p+p data from $\sqrt{s}$=5–27 GeV gives the value of $<\Delta y>$=0.7, independent of the beam energy[7].

For both Venus and RQMD, the net baryon dn/dy at midrapidity is approximately 25, but Venus displays a higher stopping power: $<\Delta y>$=3.1 units, versus 2.6 units for RQMD. The authors of RQMD emphasize the importance of baryon-meson rescattering (responsible for 25% of the stopping in RQMD) and note, " ... different y bins exhibit different physics (both in the baryon and meson sectors). It will be important to study experimentally a broad range of rapidities, not only the central rapidity slice."[3]

2.2. Meson distributions

The predictions for meson production are given in the bottom panel of Fig. 1. At issue is whether there will be in Au+Au the more or less flat "boost-invariant" plateau at midrapidity (±2 units wide) that has been observed for p+p (p+p̄) reactions over the range $\sqrt{s}$=24–900 GeV[8,9]. Also to be addressed is the question of strangeness production and the K/π ratio.

3. MINIJETS

Hard scatterings which produce "minijet" particles with $p_T > 2$ GeV/c are a probe of dense matter. Much can be learned about nuclear effects such as jet quenching and gluon shadowing from the inclusive minijet distributions[10,11]. The Hijing model[10] combines the Pythia[12] implementation of perturbative QCD for hard processes with elements of the Dual Parton Model[13] and Fritiof[1] for the soft processes. An alternative calculation is the Parton Cascade Model[14] with a cluster hadronization scheme[15]. Both of these models reproduce well the data from p+p and p+p̄ reactions at collider energies[15,16].

The predicted charged particle $dn/d\eta$ of the two models is shown in Fig. 2, with the various physical processes turned on successively, as indicated. The parton shadowing is mainly determined from the gluon nuclear structure function, about which little is presently known; the model calculations are based on quark nuclear structure functions. The STAR Experiment at RHIC plans to measure the gluon nuclear structure function via the reaction p+Au $\rightarrow \gamma$+jet [17]; after those data are obtained the model calculations may be improved. The quenching processes, too, are determined to a large extent by gluon physics, namely the induced gluon bremsstrahlung energy loss. As seen in Fig. 2, Hijing shows no effects of quenching for $\eta \geq 2$, whereas the Parton Cascade-Cluster Hadronization Model shows quenching effects to be still important for $2 \leq \eta \leq 3$.

Figure 3 shows the invariant cross-section ratio

$$R^{\mathrm{Au/p}} = \frac{\left[dn/d(p_T^2)\right]_{\mathrm{Au+Au}}}{\left[dn/d(p_T^2)\right]_{\mathrm{p+p}}} \tag{1}$$

at midrapidity versus the transverse momentum, p_T, where Au+Au and p+p are at the same beam energy per nucleon. The model dependence of this ratio is striking, and the need to measure out to, say, p_T=6 GeV/c is evident. Furthermore, the rapidity dependence of these distributions is a means of constraining the models.

4. THE BRAHMS EXPERIMENT

The BRoad Range Hadron Magnetic Spectrometers (BRAHMS) Experiment[18,19] is designed to measure identified charged hadrons ($\pi^{\pm}$, K$^{\pm}$, p$^{\pm}$) over a wide range of rapidity and transverse momentum for all beams and energies available at RHIC. Due to the different conditions at midrapidity and at more forward angles, the experiment uses two movable spectrometers for the two regions. As the layout in Fig. 4 shows, there is a Midrapidity Spectrometer to cover the laboratory polar angles $30° \leq \theta \leq 90°$ ($0 \leq \eta \leq 1.3$) and a Forward Spectrometer to cover the angles $2° \leq \theta \leq 30°$ ($1.3 \leq \eta \leq 4.0$). The Midrapidity

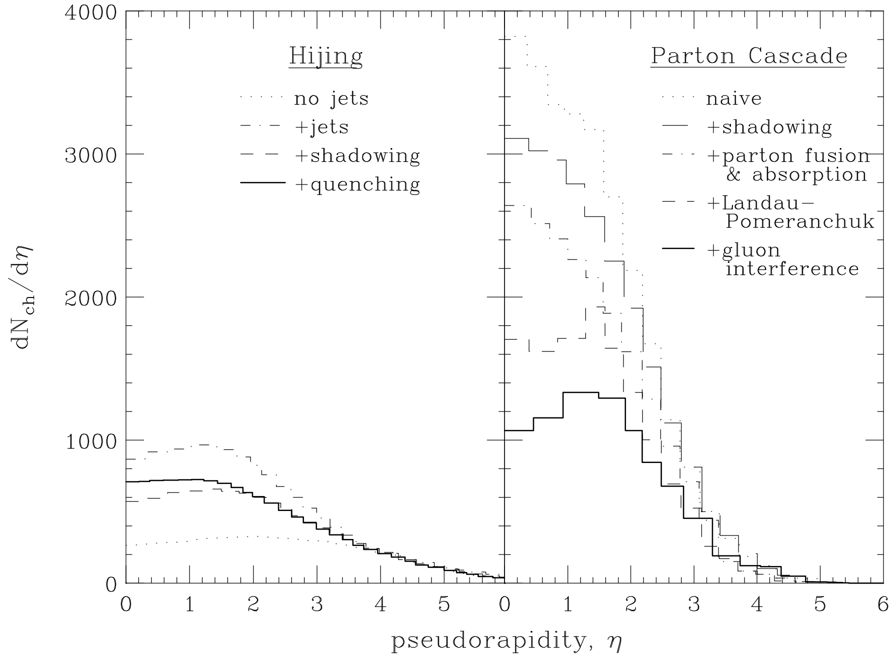

Figure 2. The charged particle distribution, $dN_{ch}/d\eta$, for central Au+Au collisions at RHIC as predicted by Hijing (left panel, from Ref. [11]) and the Parton Cascade Model (right panel, from Ref. [15]). The different curves show the effects of successively turning on various physical processes, with the full calculation given by the dark, solid histogram.

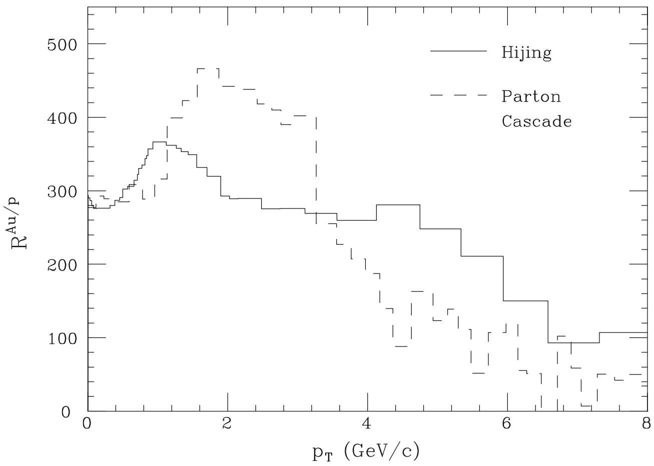

Figure 3. The ratio of the invariant cross-section from central Au+Au to that of p+p, as a function of p_T, from Hijing (Ref. [11]) and the Parton Cascade Model (Ref. [15]). Both reactions are at a c.m. energy of 200 GeV per nucleon pair.

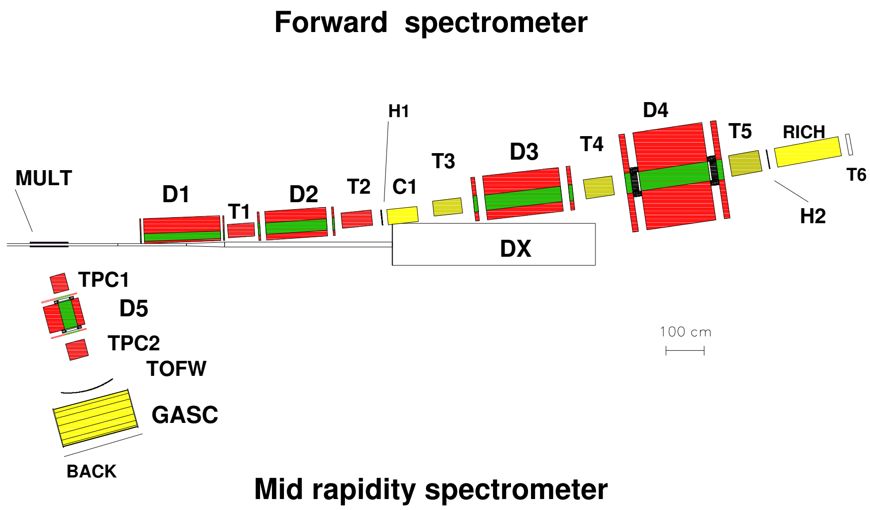

Figure 4. Plan view of the BRAHMS spectrometers. Both spectrometers are freely rotating: the forward arm is shown at θ=2° and the midrapidity arm at 75°. DX is the RHIC final focusing beam magnet.

Spectrometer is described in the contribution to these proceedings by D. Beavis[20], and is not discussed further here. Greater detail on all aspects of BRAHMS may be found in the Conceptual Design Report[19].

The Forward Spectrometer employs four dipole magnets, D1–D4, each of which has a maximum bending power of 2.4 T-m. D1 has a septum design, in order to allow positioning as close as possible to the beampipe, and has a fringe field on the collider beam of only 7 gauss. Tracking is performed by time projection chambers T1, T2 and T3, followed by drift chambers T4 and T5. Particle identification is achieved with time-of-flight hodoscopes H1 (at 9 m from the vertex) and H2 (at 20 m from the vertex), threshold Čerenkov counter C1 and ring-imaging Čerenkov counter RICH. The Forward Spectrometer moves in two pieces: the front arm consisting of D1–C1 can rotate over the range $2°\leq\theta\leq30°$ $(1.3\leq\eta\leq4.0)$, whereas the full spectrometer D1–T6 is restricted to $2°\leq\theta\leq15°$ $(2.0\leq\eta\leq4.0)$. The solid angle acceptance of the spectrometer is 0.8 msr.

BRAHMS also has a silicon strip multiplicity detector, MULT, which is based on the design of the PHOBOS vertex detector[21]. MULT covers the region $|\eta|\leq2.5$ and provides the first-level centrality trigger for the experiment. The start signal for the time-of-flight system will come from beam-beam counters (not shown in Fig. 4) which will also perform a crude vertex position determination.

4.1. Acceptance of BRAHMS

The overall acceptance in $(y,\ p_T)$ space of pions, kaons and protons for BRAHMS is shown in Fig. 5. The total BRAHMS rapidity coverage is $0 \leq y \leq 3.5$ for protons and $0 \leq y \leq 4.0$ for mesons (c.f. Fig. 1). To emphasize how the broad coverage of BRAHMS contributes to the RHIC program, the single pion acceptances of the four baseline RHIC

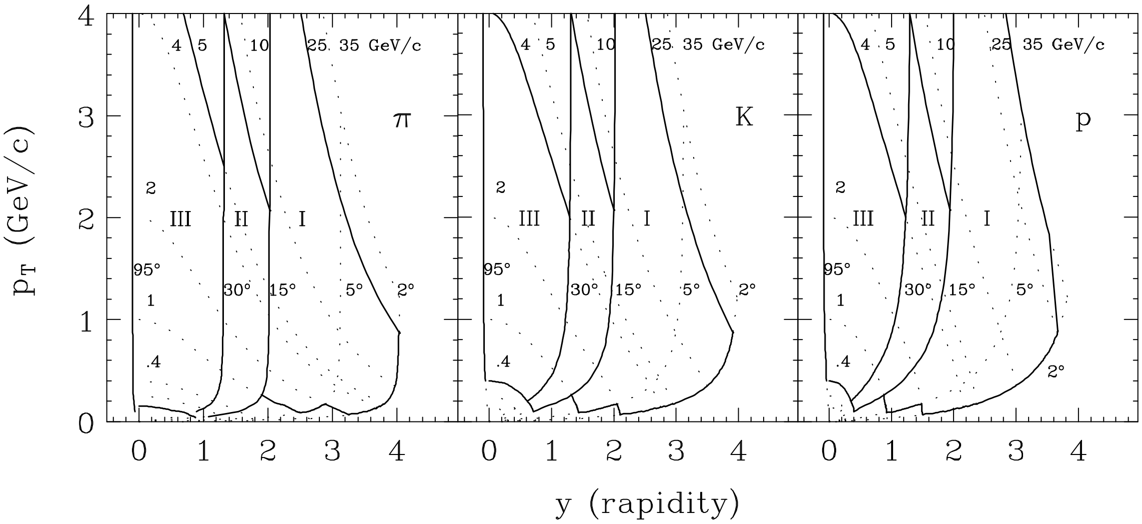

Figure 5. The acceptance of BRAHMS in (y, p_T) space for pions (left frame), kaons (middle frame) and protons (right frame). Region I is with the full Forward Arm, Region II is for the D1–C1 section of the Forward Arm alone, and Region III is with the Midrapidity Arm.

experiments are compared in Fig. 6.

4.2. Expected track density

The expected charged particle multiplicities in the Forward Spectrometer tracking chambers for different momentum settings are given in Table 1. The worst case of θ=2° and the model Venus is taken, yet the particle densities of $\leq$0.04 cm^{-2} do not present a major experimental difficulty.

4.3. Particle identification

The regions of π/K and K/p separation for the various particle identification counters are shown in Fig. 7. The time-of-flight discrimination is set at the 4σ level, where σ = 75 ps is the rms timing resolution. The highest momenta are covered by the RICH counter: π/K up to p=25 GeV/c and K/p up to p=35 GeV/c. Data from successful in-beam tests of a prototype RICH counter with a multianode photomultiplier readout[22] are presented in Fig. 8.

5. COUNTING RATES IN THE FORWARD SPECTROMETER

Event-generating models have been used to estimate the counting rates in the Forward Spectrometer for central Au+Au collisions. Table 2 lists the running time necessary to get high quality soft particle spectra, allowing for accurate determinations of the slope parameter, etc. Fritiof is used since this gives the lowest rates, and 50 events/sec is assumed. The full soft physics program will require about half a year at the RHIC design

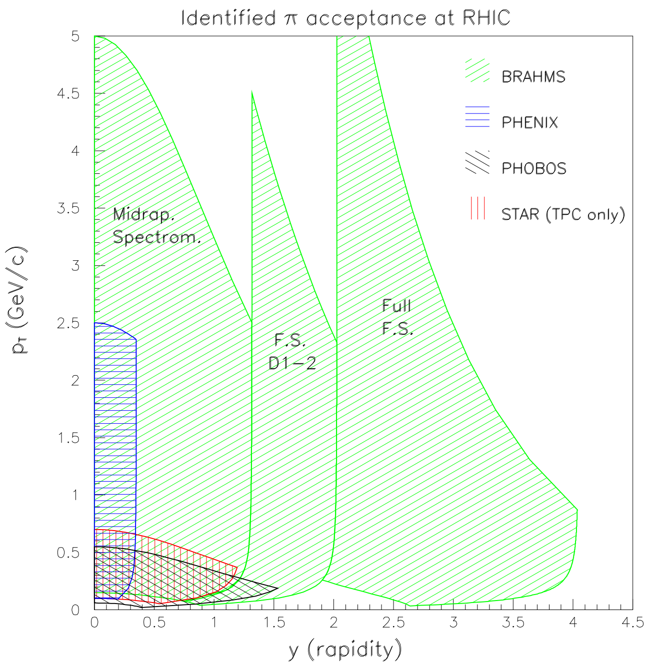

Figure 6. The identified pion acceptance for the four baseline RHIC experiments.

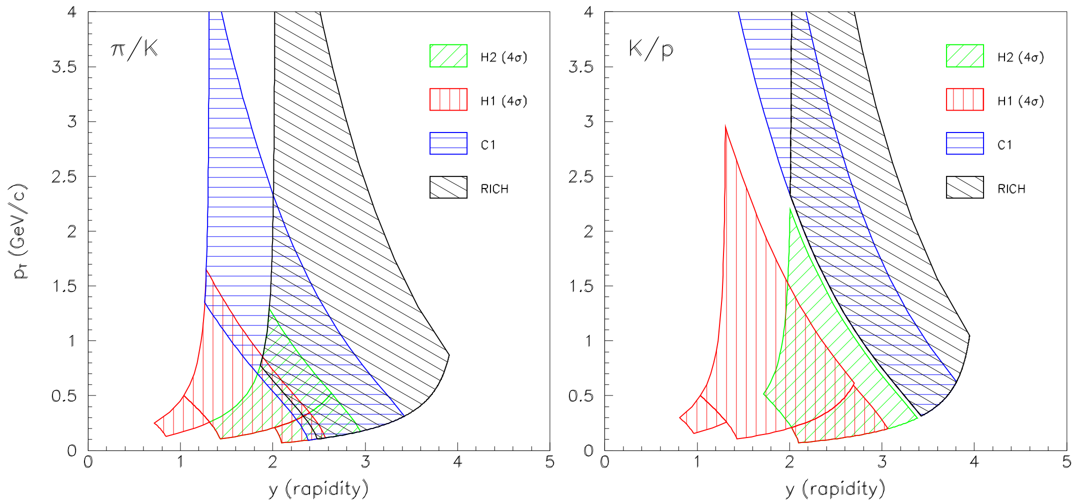

Figure 7. Coverage of the various particle identification counters in the BRAHMS Forward Spectrometer. The left panel shows the π/K separation and the right panel shows K/p.

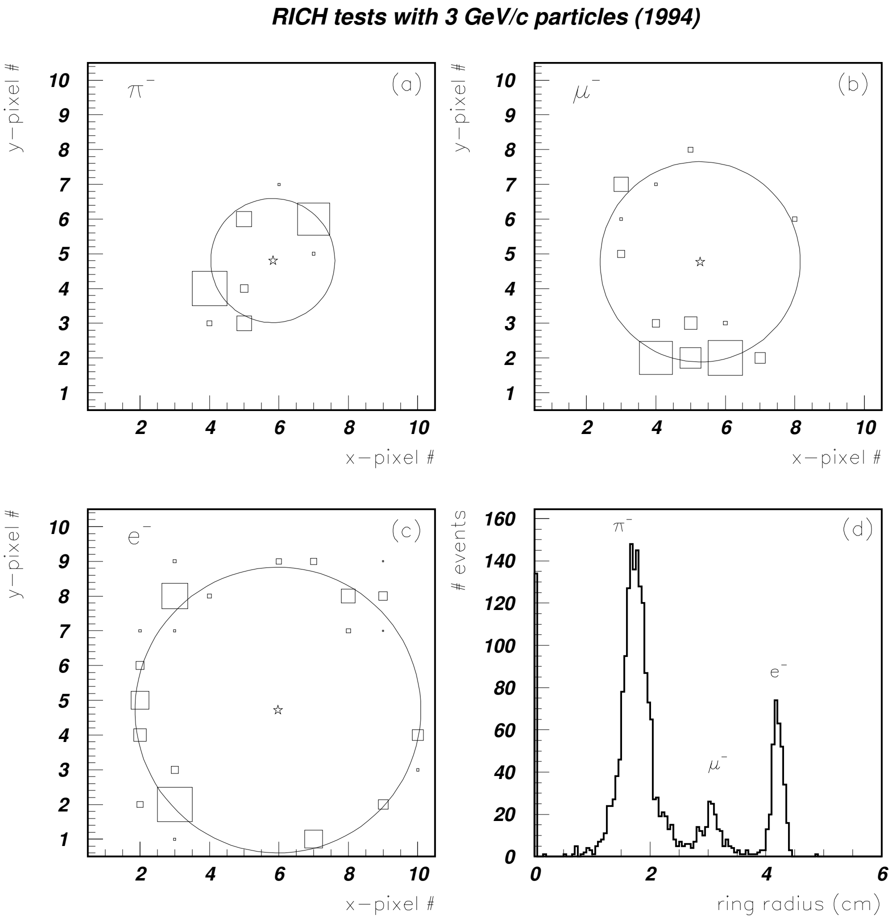

Figure 8. Results from Ref. [22] for a prototype RICH counter with a test beam of 3 GeV/c negative particles. Panels a, b and c show individual events with fitted rings; the ring centers are shown as stars and come from independent drift chamber tracking. Panel d is a histogram of the fitted ring radius from the entire run, showing peaks identified as π^-, μ^- and e$^-$.

luminosity.

A similar listing of running times for the minijet inclusive spectrum is found in Table 3. In this case, the demands on the statistics are not as strict as they were for the soft spectra, and we are willing to set a large p_T bin size (0.5 GeV/c). The table uses the predictions of Hijing, but Fritiof gives similar results. A minimum measurement to p_T=6 GeV/c at y=2 will require about one week of running time. BRAHMS will also be able to identify the minijet particle specie, allowing for "flavor tagging".

6. SUMMARY AND OUTLOOK

In conclusion, it should be emphasized that BRAHMS will be ready to take data on the day that RHIC turns on, and will handle all beams and energies. The broad range of data measured by the BRAHMS Experiment will provide extensive constraints on the conflicting models and will lead to a better understanding of the conditions produced in RHIC collisions.

7. ACKNOWLEDGEMENTS

I am grateful to my colleagues J.H. Lee, D. Beavis and F. Videbæk for their help in preparing the figures for this paper. W. Christie kindly provided the Hijing events used in the minijet rate calculation. Finally I thank the organizers, T. Hallman and J. Thomas, for all their efforts in making this workshop a reality.

REFERENCES

1. B. Andersson, G. Gustafson and B. Nielsson-Almqvist, Nucl. Phys. B281 (1987) 289.
2. K. Werner, Z. Physics **C42** (1989) 85.
3. Th. Schönfeld, H. Stöcker, W. Greiner and H. Sorge, Mod. Phys. Lett. **A8** (1993) 2631.
4. Th. Schönfeld *et al.*, Nucl. Phys. **A544** (1992) 439c.
5. H. Sorge, private communication (1995).
6. W. Busza and A.S. Goldhaber, Phys. Lett. **B139** (1984) 235; W. Busza and R. Ledoux, Ann. Rev. Nucl. Part. Sci. **38** (1988) 119. Unfortunately, this type of analysis has not yet been extended to collider energies.
7. F. Videbæk, private communication (1995).
8. W. Thomé *et al.*, Nucl. Phys. **B129** (1977) 365.
9. UA5 Collaboration, G.J. Alner *et al.*, Z. Phys. **C33** (1986) 1.
10. X.N. Wang and M. Gyulassy, Phys. Rev. **D44** (1991) 3501.
11. X.N. Wang and M. Gyulassy, Phys. Rev. Lett. **68** (1992) 1480.
12. T. Sjöstrand and M. van Zijl, Phys. Rev. **D36** (1987) 2019.
13. A. Capella, U. Sukhatme and J. Tran Tranh Van, Z. Phys. **C3** (1980) 329.
14. K. Geiger and B. Müller, Nucl. Phys. **B369** (1992) 600.
15. K. Geiger, Phys. Rev. **D47** (1993) 133.
16. X.N. Wang and M. Gyulassy, Phys. Rev. **D45** (1992) 844.
17. W. Christie, contribution to this volume.
18. F. Videbæk, Nucl. Phys. **A566** (1994) 299c.
19. K. Ashktorab *et al.*, BRAHMS Conceptual Design Report, Brookhaven National Laboratory (1994). This document is also available through the World Wide Web at address http://rsgi01.rhic.bnl.gov/export1/brahms/WWW/cdr/cdr.html.
20. D. Beavis, contribution to this volume.
21. D. Barton *et al.*, PHOBOS Conceptual Design Report, Brookhaven National Laboratory (1994).
22. R. Debbe *et al.*, BNL-61218, to be published in Nucl. Instrum. and Methods A (1995).

Table 1
Expected average charged particle multiplicities per event in the tracking chambers of the Forward Spectrometer, from GEANT simulations with 400 central Au+Au Venus events. The θ=2.1° angular setting for the spectrometer is assumed.

Momentum setting	Detector	# primaries	# secondaries	Total #	Density (particles/cm^2)
2–5 GeV/c	T1	6.6	10.0	16.5	0.04
"	T2	2.4	1.4	3.8	0.01
7.5–15 GeV/c	T2	4.1	3.5	7.6	0.02
"	T3	2.7	4.4	7.1	0.007
"	T4	1.5	0.8	2.4	0.002
"	T5	1.0	0.5	1.6	0.001
15–30 GeV/c	T2	2.2	2.5	4.7	0.01
"	T3	1.2	4.6	5.9	0.006
"	T4	0.6	1.0	1.6	0.001
"	T5	0.3	0.5	0.8	0.0004

Table 2
Counting rates for the soft physics spectra in the BRAHMS Forward Spectrometer for Au+Au central collisions, assuming 50 events/sec are written to tape. The model used is Fritiof 1.7 and 1000 π^+ are required to be in the highest p_T bin, with a bin size of 40 MeV/c.

Angle θ	Highest p_T bin (GeV/c)	p_{max} (GeV/c)	counts/collision in bin	time at p_{max} (hrs.)	total time at angle (hrs.)
3°	1.26-1.30	25	3×10^{-3}	2	3
5°	1.96-2.00	23	5×10^{-4}	12	20
10°	1.96-2.00	12	3×10^{-4}	18	28
15°	1.96-2.00	8	1×10^{-4}	56	80

Table 3
Counting rates for minijets in the BRAHMS Forward Spectrometer for Au+Au central collisions, assuming 50 events/sec are written to tape. The model used is Hijing 1.0 and 100 protons are required to be in the highest p_T bin, with a bin size of 0.5 GeV/c.

Angle θ	Highest p_T bin (GeV/c)	p_{max} (GeV/c)	counts/collision in bin	time at p_{max} (hrs.)
15° (y=2)	4.5-5.0	19	8×10^{-6}	70
15° (y=2)	5.5-6.0	23	3×10^{-6}	160